Received: 1 May 2022 | Revised: 19 July 2022 | Accepted: 10 August 2022

DOI: 10.1002/pc.27001

RESEARCH ARTICLE

Polymer COMPOSITES WILEY

Controlling resin flow in Liquid Composite Moulding processes through localized irradiation with ultraviolet light

Andreas Endruweit[1] | **Mikhail Matveev**[1] | **Michael V. Tretyakov**[2]

[1]Composites Research Group, Faculty of Engineering, University of Nottingham, Nottingham, UK

[2]School of Mathematical Sciences, University of Nottingham, Nottingham, UK

Correspondence
Andreas Endruweit, Composites Research Group, Faculty of Engineering, University of Nottingham, Nottingham, UK.
Email: andreas.endruweit@nottingham.ac.uk

Funding information
Engineering and Physical Sciences Research Council, Grant/Award Number: EP/P006701/1

Abstract

A vacuum infusion process was implemented to produce composite specimens from a random glass filament mat and an acrylic modified polyester resin curable upon irradiation with ultraviolet (UV) light. Through localized irradiation with UV light during the reinforcement impregnation, the viscosity of the flowing resin was increased selectively. This allowed converging–diverging flow patterns with defined inclusions to be realized and racetracking along reinforcement edges to be suppressed. The approach is based on radical photopolymerisation. Here, the degree of cure and the viscosity of the resin increase under direct irradiation, such that the resin gels and the flow stalls in a matter of seconds, but remain unchanged in areas covered with an opaque mask. While this study is concerned with the feasibility of the process, potential practical applications are in flow control for Liquid Composite Moulding, that is, compensation for local variations in the fiber volume fraction and permeability of reinforcements.

KEYWORDS

Liquid Composite Moulding, resin cure, resin flow, ultraviolet light, viscosity

1 | INTRODUCTION

In Liquid Composite Moulding (LCM) processes, a dry fibrous reinforcement is placed in some form of tooling which applies a compaction pressure onto the reinforcement surface. The reinforcement is then impregnated with a liquid thermoset resin, upon application of a flow-driving pressure gradient. Once the reinforcement is impregnated, it is left in the tool until cure of the resin is complete. The composite component can then be removed from the tool and finished.

An important characteristics of LCM processes is that long-range resin flow develops during the reinforcement impregnation. The flow front, which separates the dry from the wetted part of the reinforcement, propagates at a velocity described by

$$\mathbf{v}_f = -\frac{\mathbf{K}}{\Phi\eta}\cdot\nabla p. \tag{1}$$

Here, $\mathbf{K}$ is a second-order tensor describing the (directional) permeability of the reinforcement, Φ is the porosity of the reinforcement, η is the viscosity of the resin, and ∇p is the gradient in fluid pressure. The porosity is related to the fiber volume fraction, V_f, through

$$\Phi = 1 - V_f. \quad (2)$$

The permeability, **K**, is a function of Φ and also depends on the fiber arrangement in the reinforcement.[1] The viscosity of a thermoset can be described as a function of the temperature and degree of cure. The pressure gradient depends on the pressure applied at resin inlets and vents and the lay-out of the tooling. The flow front propagation determines the quality of the component (in terms of complete reinforcement impregnation) and the process cycle time.

A well-known practical problem is the local variability in fiber arrangement (also orientation) and fiber volume fraction,[2] which is related to reinforcement deformation during forming (drape)[3] and to stochastic reinforcement variability.[4] This implies that Φ and **K** also vary locally, which can result in irregular resin flow patterns. Dry spots may form, particularly if a low-permeability zone is surrounded by high-permeability zones.

Another effect that has a strong influence on the resin flow in LCM processes occurs if the fit of the reinforcement to the tool cavity is poor. This results in the formation of empty channels along the reinforcement edges, where the flow front velocity is higher than in the reinforcement ("racetracking").[5] The flow channels are commonly characterized by an equivalent permeability, defined as the ratio of flow velocity and pressure drop along the length of the channel (and for a fluid with given viscosity).[6] Similarly, bending of the reinforcement around geometry edges results in local compression, that is, reduced permeability, on the inside of the bend and formation of a gap, that is, racetracking, on the outside,[7] particularly for multi-layer reinforcement. This results in through-thickness variations in the flow front propagation.

To minimize effects of local variability in Φ and **K**, in-process control of the flow front propagation is generally desirable,[8–10] particularly if the true local distribution of porosity and permeability can be estimated with good accuracy based on process data.[11] As the flow front velocity depends on the pressure gradient, it can be controlled through variation of the pressure at inlets and vents, control of resin flow through inlets with fixed location,[12] or selection of inlet locations.[13] However, the pressure gradient affects resin flow globally (everywhere between inlet and vent), with limited local controllability.[9]

Local control of Φ (and hence **K)** is possible in processes such as Vacuum Infusion (VI), where the reinforcement is enclosed in a flexible vacuum bag. To increase Φ locally for the duration of the infusion process, application of vacuum on the outside of the vacuum bag has been proposed, which relaxes the pressure compacting the reinforcement.[14] As an alternative, electromagnetic actuation of the vacuum bag has been applied to modify the porosity locally.[15]

Equation (1) also implies that local variations in **K**/Φ can be compensated for by varying η locally by the same factor. As the resin viscosity depends on the temperature, reducing it through localized heating has been proposed.[16,17] However, heat conduction in the composite and in the tooling makes it difficult to control the temperature and reduce the viscosity locally. It is also to be considered that there are interdependencies between the temperature and the curing rate for thermosetting resins. Increasing the temperature to reduce the viscosity will also result in an increased curing rate, that is, a faster increase in resin viscosity, which limits the time window for the flow process. As an alternative, resin systems could be used that cure when exposed to light, particularly ultraviolet (UV) light, but not when heated. If a suitable resin system is selected, it can be cured locally to increase the viscosity where it is exposed to light and kept uncured where it is shielded from irradiation.[18] In addition, the temperature can be increased (globally) to reduce the viscosity without inducing the curing process.

Here, a LCM process is combined with selective UV curing to study the effect of local increases in the resin viscosity on the flow front propagation and assess the feasibility of controlling resin flow through localized irradiation.

2 | THEORY

2.1 | Basics of UV curing

The mechanisms of UV curing are discussed extensively in the literature (e.g., by Decker[19] or Green[20]). The most widely used UV-curable resins are based on acrylates, which undergo free radical polymerization. Upon irradiation with UV light, a photoinitiator, which is added to the base resin at a defined concentration, is decomposed to produce free radicals. Bonding of a radical to a monomer initiates a continuous chain growing reaction, as this creates a new monomer radical. Addition of monomers propagates until all monomers are bonded, or until the chain growth is terminated through a reaction of a polymer chain radical with another radical.

Since free radicals are only produced when the photoinitiator is exposed to UV light, the polymerization ceases because of radical–radical termination reactions as soon as the irradiation stops. Hence, the resin cures only under direct irradiation and remains uncured in the shadow. The free radical polymerization is also inhibited in the presence of oxygen, as oxygen reacts with the radicals. This effect can be overcome by performing the curing process in a vacuum or in an inert atmosphere.

In composites manufacture, the characteristics of UV-curable resin systems imply that reinforcement fibers need to be transparent to UV light to obtain through-thickness cure of the resin. On the other hand, they allow the reinforcement impregnation and the resin cure to be completely separated. This can be an advantage, particularly in LCM processes. As long as the resin is not exposed to UV light during impregnation of the reinforcement, the degree of cure (i.e., the viscosity) does not increase, and there is no risk of premature gelation. Once the reinforcement impregnation is complete, the resin can be irradiated and cured. The resin can also be heated to reduce the viscosity during processing and to aid the impregnation of the reinforcement. Whilst this has no direct effect on the curing process or the properties of the finished product, increased molecular mobility allows higher curing rates to be obtained when a heated resin is irradiated with UV light.

As direct irradiation of the laminate is required for UV curing, it is primarily used for open mold processes such as wet lay-up. UV curing can also be applied to VI processes,[21–23] as long as the membranes used for vacuum bagging are not opaque to UV radiation. As vacuum is applied in these processes, the radical polymerization is not inhibited by oxygen. UV-curable resins have also been used in prepregs,[21,24] and for "on the fly" curing in continuous processes, such as filament winding,[25] braiding with on-line impregnation,[26,27] and pultrusion.[28]

For joining of composite components, it has been proposed to prevent the bonding surface of an uncured laminate, that is, of a fully impregnated reinforcement, from curing by selectively covering it with an opaque film while the rest of the laminate is exposed to UV irradiation. After removal of the opaque film, a second (partially) uncured laminate can be overlapped onto the uncured laminate section. Subsequent curing of the overlap results in a joint based on a primary bond instead of a secondary bond ("wet edge" lamination[21]).

For other resins (e.g., epoxies), UV curing is based on a different mechanism, namely cationic polymerization. Once the cationic polymerization process has started, it will continue after the UV irradiation ends ("shadow curing"). This also implies that an entire component will cure, even if not all parts are directly exposed to UV irradiation.[19,20] For the purpose of this study, these resins are less suitable, as controllability of the curing process through local irradiation is lost.

2.2 | Degree of cure and viscosity

The degree of cure, α, of a UV-curable resin system depends on the radiant exposure, H, which is the total radiant energy incident on a surface per unit area. This dependence can be approximated by a relation of the type

$$\alpha = 1 - \exp(-H/H_0), \tag{3}$$

where, H_0 is a material constant.[29] The radiant exposure is derived from the irradiance, E, that is, the radiant power incident on a surface per unit area, by integration over the irradiation time, t. If the irradiance is constant, H can be expressed as

$$H = Et. \tag{4}$$

The irradiance is related to the emittance of a light source, that is, the radiant power emitted from a surface per unit area, and geometrical factors. It drops exponentially with increasing distance from the light source and with increasing attenuation coefficient of the medium the light travels through (Beer–Lambert law). If the normal of an irradiated surface and incident light rays include an angle, θ, the irradiance is proportional to $\cos\theta$. It is to be noted that emittance, irradiance and radiant exposure, as well as the attenuation coefficient of a medium, are spectral quantities, that is, they can have different values at different wavelengths.

In general, the viscosity of polymers depends on the degree of cure (which is related to the molecular mass), temperature, and shear rate. However, at the low flow velocities (i.e., low shear rates) occurring in most LCM processes, the dependence on the shear rate is weak and can be neglected. The resins exhibit approximately Newtonian behavior. For thermoset resins, the characteristics of the viscosity, η, relevant to composites processing are a decrease with increasing temperature, T, and an increase with increasing degree of cure, α. Both are captured in a variety of models proposed in the literature for different resin systems.[30]

Here, the degree of cure and the resin temperature of a UV-curable resin are considered independent of each other. Adapting a simple model,[31] the increase in viscosity with increasing degree of cure (i.e., with radiant exposure or duration of irradiation) at a constant temperature is approximated as

$$\eta(\alpha, T) = \eta_T \exp(c\alpha), \tag{5}$$

where, η_T expresses the dependence on the temperature at $H = 0$, and the factor c is assumed to be independent of the temperature.

2.3 | Resin flow with irradiation

The pressure-driven flow of a UV-curable resin under UV irradiation can be described by combining Equation (1)

with Equation (5). As the resin is flowing, the degree of cure does not only depend on the time, as expressed in Equations (3) and (4), but also on the position. The local change in the degree of cure is

$$\frac{d\alpha}{dt}=\frac{\partial\alpha}{\partial t}+\mathbf{v}\nabla\alpha. \tag{6}$$

Here, the first term on the right-hand side relates to the curing reaction. The second term relates to advection, that is, resin with a certain degree of cure flowing at a velocity, $\mathbf{v}$, in the presence of gradients in the degree of cure. This means that the resin viscosity also depends on position and time.

The effect of the irradiation on the flow front propagation is illustrated here for one-dimensional flow (in direction x), where x_f is the length covered by the moving flow front and Δp is the pressure drop between resin inlet and flow front. For this case, Equation (1) can be expressed as

$$\frac{dx_f}{dt}=-\frac{K}{\Phi\eta}\frac{\Delta p}{x_f}. \tag{7}$$

The following assumptions are made to simplify the problem for illustration:

- The reinforcement porosity and permeability are uniform and constant, as would be the case for ideal reinforcements with uniform fiber arrangement and LCM processes with rigid tooling and given reinforcement thickness, such as Resin Transfer Moulding.
- The temperature is constant.
- The irradiance does not vary while the resin is flowing.
- The pressure drop between resin inlet and vent is constant.

The flow front position as a function of the time can be found by integrating Equation (7). As η depends on x (between 0 and x_f) and t, the problem was solved numerically. Typical results are plotted in Figure 1, where it is assumed that the entire resin flow domain is irradiated and the input values listed in Table 1 are used. Qualitatively, the increase in viscosity between the resin inlet and the flow front results in a decrease in flow velocity (which, in 1D flow, is the same everywhere in the flow domain). Eventually, the resin gels, and the flow stalls at a maximum flow length, which

- decreases if Δp, and hence the pressure gradient driving flow in the given time prior to gelation, is reduced (Figure 1A);
- decreases if E is increased, that is, the time to gelation is reduced (Figure 1B);
- increases if T is increased, that is, the initial viscosity is decreased and the initial flow velocity is increased prior to gelation (Figure 1C).

Here, different solutions are compared based on the flow front positions at a viscosity of 100 Pa s, which is assumed to correspond to the flow limit. The pressure distributions plotted in Figure 1 relate to these flow front positions.

In the case shown in Figure 2, the resin is assumed to be shielded from irradiation in a part of the flow domain (with length, l_m), where $E = 0$ and $\eta = \text{const}$, and irradiated in another part, where $E > 0$ and the viscosity increases. In this case, the total flow time and the time for the degree of cure to change are not the same, which needs to be considered when integrating Equation (7). The maximum flow length in the exposed part of the flow domain, that is,

$$\Delta x_f = x_f - l_m, \tag{8}$$

is 10 mm and 6 mm for values of l_m of 15 mm and 38 mm, respectively. This decrease in Δx_f with increasing l_m is consistent with Figure 1A, as an increase in l_m means that the effective pressure drop, Δp, between the end of the mask and the flow front is reduced.

3 | MATERIALS AND METHODS

3.1 | LCM experiments

This study is based on a VI process with UV curing, as it is easy to implement. A continuous glass filament mat with random fiber orientation (Unifilo) and a measured superficial density of approximately 220 g/m^2 was used as reinforcement. It was impregnated with a commercial resin (Solarez® acrylic modified polyester) to form a composite. Unless stated otherwise, reinforcement specimens were rectangular with a length, l, of 280 mm and a width, w, of 115 mm, and consisted of six layers of the glass fiber mat. A nylon film with 50 µm thickness was used as vacuum bag. Polypropylene flow mesh was placed along the short edges of the specimens to create a linear resin inlet and a linear vent (Figure 3A). If the material properties of the reinforcement (and of the resin) are uniform, this configuration results in uni-directional flow. As no flow medium (and peel ply) was used on top of the reinforcement, it can be assumed that pure in-plane flow develops during the infusion process. For curing, a UV light source was placed over the vacuum bag at a height, h (Figure 3B). In all experiments with combined resin flow and local curing (Section 4), the light source was

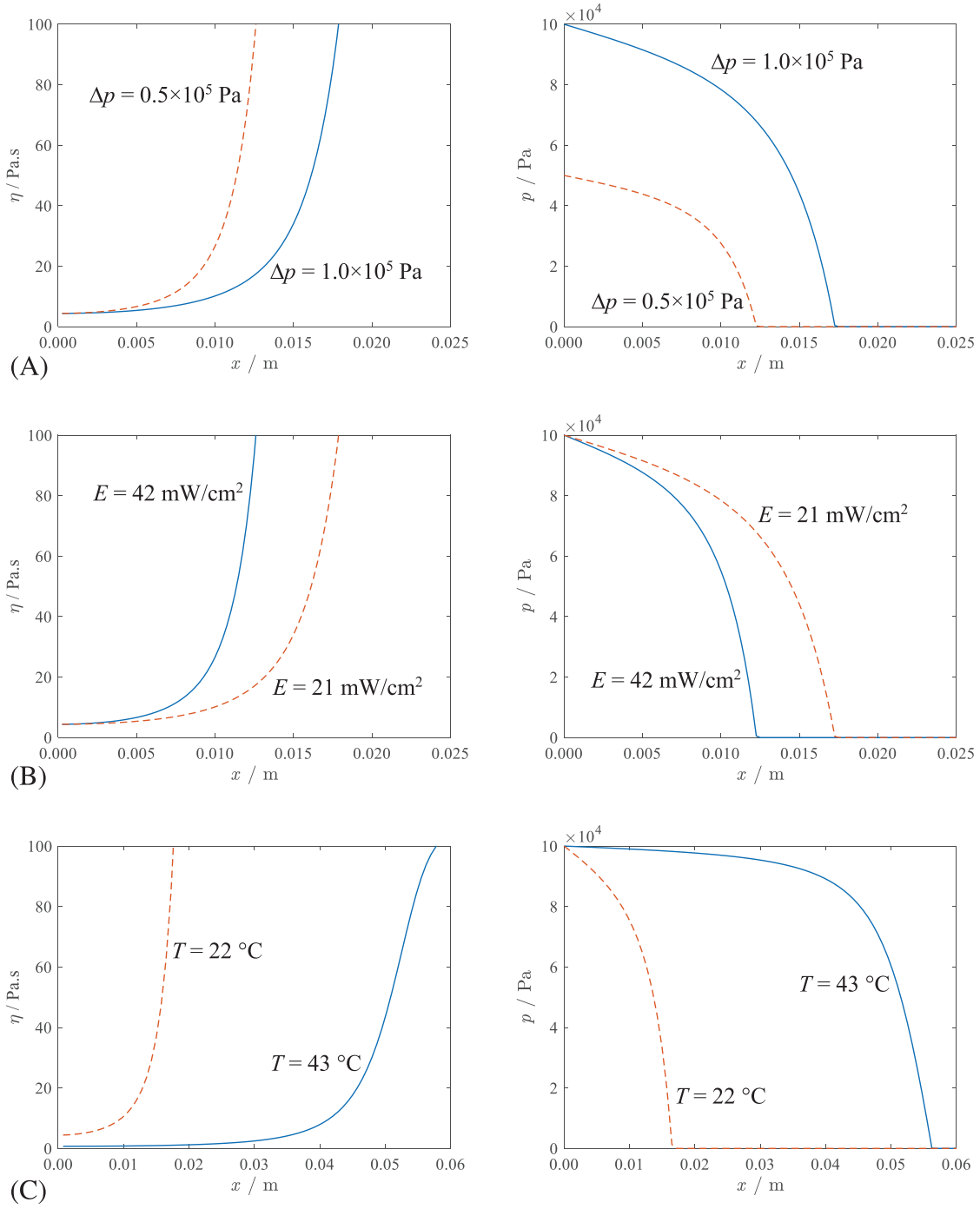

FIGURE 1 Numerical solution of resin flow problem with UV irradiation, 1D case: Resin viscosity, η, and pressure, p, as a function of the position along the flow direction, x; (A) at different pressure drop, Δp, and $E = 21$ mW/cm^2, $T = 22$°C; (B) at different irradiance, E, and $\Delta p = 1.0 \times 10^5$ Pa, $T = 22$°C; (C) at different temperature, T, and $\Delta p = 1.0 \times 10^5$ Pa, $E = 21$ mW/cm^2

TABLE 1 Input values used in the numerical solution of Equation (7).

		Δp (10^5 Pa)		η_T (Pa s)		E (mW/cm^2)			
K (10^{-10} m^2)	Φ	High	Low	$T = 22$°C	$T = 43$°C	High	Low	H_0 (mJ/cm^2)	c
8	0.77	1.0	0.5	4.39	0.71	42	21	286	5

Note: The values for K, Φ, Δp, η_T, and E were selected to approximate values in experiments (Sections 3 and 4); H_0 was estimated based on curing experiments discussed in Section 3; c was chosen so that the flow length is of the same order of magnitude as observed experimentally (Section 4).

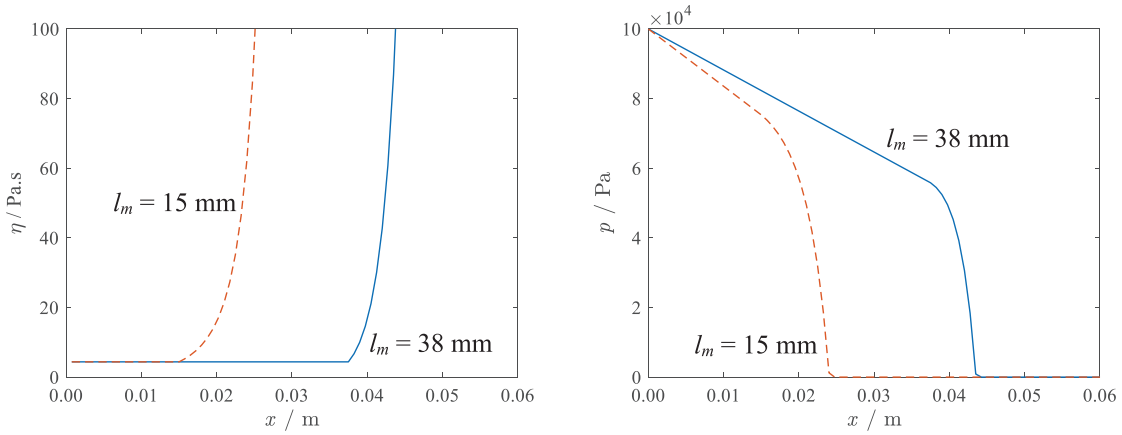

FIGURE 2 Numerical solution of resin flow problem with UV irradiation and mask, 1D case: Resin viscosity, η, and pressure, p, as a function of the position along the flow direction, x, at different length of the mask, l_m, and $\Delta p = 1.0 \times 10^5$ Pa, $E = 21$ mW/cm^2, $T = 22°$C

switched on for the entire duration of the infusion process.

3.2 | UV irradiation

The light source used for irradiation of the vacuum bag is a 400 W flood light (Dymax 2000 PC) with a metal halide "D" bulb. Major emission peaks of the bulb lie at wavelengths of approximately 365 and 440 nm, that is, in the UV-A and visible blue range of the electromagnetic spectrum. The lamp has a rectangular reflector housing with an opening of dimensions 26.7 cm × 22.9 cm. For measurement of the irradiance, E, in the UV-A band, a UV201-UVA Radiometer (Macam Photometrics Ltd.) with a responsivity peak at 365 nm and a full width at half maximum of (35 ± 2) nm was used. The minimum resolution of this instrument is 0.1 mW/cm^2. Here, the irradiance on the surface of the vacuum bag was set by adjusting the height of the lamp, h, to approximately 20 cm. As shown in Figure 4, the irradiance measured at this height (along the long axis of the rectangular reflector) drops from the center towards the edges of the lamp reflector, following a parabolic profile which can be approximated by

$$E(h = 20\text{ cm}) = \left(-3.13 \times 10^{-2} \left(\frac{x}{\text{cm}}\right)^2 - 0.29 \times 10^{-2} \left(\frac{x}{\text{cm}}\right) + 30.25 \right) \text{mW/cm}^2. \quad (9)$$

This implies that, over the length of a 28 cm long specimen, the irradiance decreases by approximately 20% from the center to the ends (at $x = \pm 14$ cm).

In infusion experiments with selective local irradiation, masks cut from corrugated cardboard were placed on the surface of the vacuum bag to shield defined areas from UV light. To avoid curing of resin in the feed line and vacuum line during the infusion process, both were wrapped in aluminum foil. The light transmission of all materials used in this study was determined according to

$$\tau = \frac{E_t}{E_0}, \quad (10)$$

where the irradiance without material, E_0, and with material, E_t, were measured at a given distance from the light source.[32] Values of the transmission in the UV-A band are listed in Table 2.

To determine the transmission of six layers of the impregnated and compacted reinforcement, an infusion was carried out on a glass plate with a thickness of 10 mm. In the center of the specimen, the irradiance on the surface of the vacuum bag is approximately 30.3 mW/cm^2 (Figure 4). As the transmission through one layer of vacuum bag is 82%, the irradiance on the top surface of the impregnated reinforcement is approximately 24.6 mW/cm^2. The irradiance underneath the glass plate was found to be below the measurable value of 0.1 mW/cm^2. Taking into account the transmission of the glass plate (77%), it can be concluded that the irradiance on the bottom surface of the impregnated reinforcement is also in the order of 0.1 mW/cm^2 and that the transmission of the lay-up is lower than 1%.

3.3 | Resin properties

A Brookfield viscometer (DV II+) was used to measure the viscosity of the uncured resin (at $H = 0$) in the

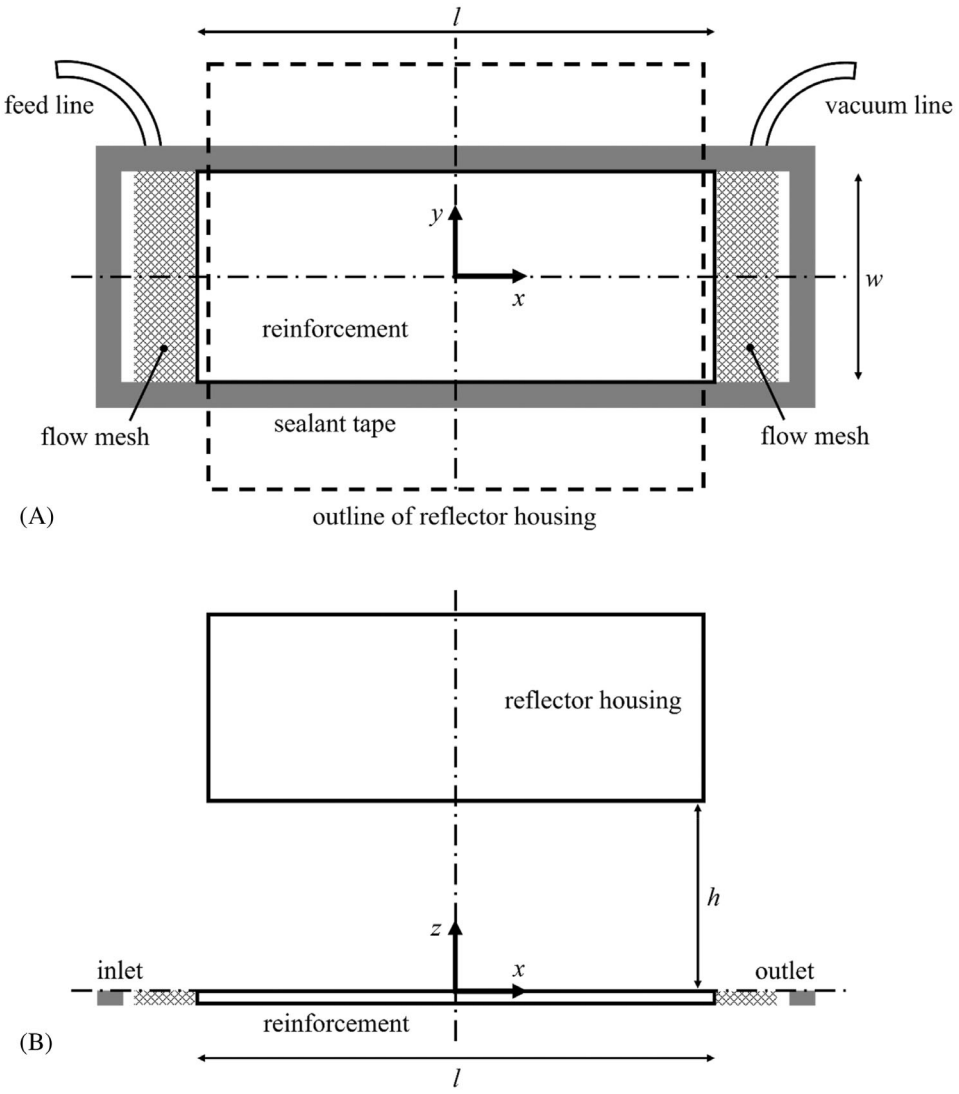

FIGURE 3 Experimental set-up for vacuum infusion experiments with UV irradiation: (A) top view; (B) side view

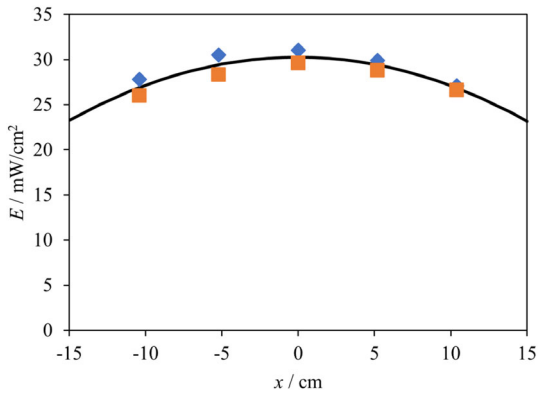

FIGURE 4 Irradiance at a vertical distance $h = 20$ cm from the lamp reflector housing, measured along two lines at a distance $y = \pm 2.9$ cm (square and diamond markers) from the center axis. The solid line indicates the approximation described by Equation (9)

TABLE 2 Transmission, τ, in the UV-A band (365 nm responsivity peak), measured for different materials

Material	τ (%)
Corrugated cardboard	0
Aluminum foil, 10 μm thick, shiny face up	0
Aluminum foil, 10 μm thick, dull face up	0
Nylon vacuum bag, 50 μm thick, 1 layer	82
Nylon vacuum bag, 50 μm thick, 2 layers	67
Polypropylene flow mesh, 4 layers	~68
Glass filament mat, 1 layer, dry, not compacted	20–33
Glass filament mat, 2 layers, dry, not compacted	3–7
Glass filament mat, 3 layers, dry, not compacted	<1
Glass filament mat, 6 layers, impregnated with resin and compacted in vacuum bag	<1
Glass plate, 10 mm thick	77

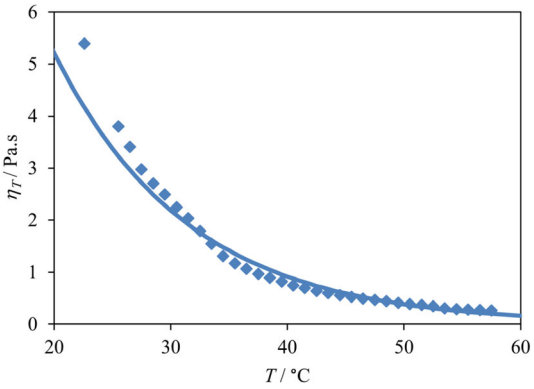

FIGURE 5 Resin viscosity, η_T, as a function of the resin temperature, T, at a radiant exposure $H = 0$. Diamond markers indicate experimental data, the solid line is a fit described by Equation (11). The coefficient of correlation is $R^2 = 0.972$

temperature range between 20 and 60°C. The results can be represented by the fitted curve

$$\eta_T = 29.7\,\text{Pa s} \times \exp\left(-0.087 T/^{\circ}\text{C}\right), \qquad (11)$$

which is plotted in Figure 5. It is to be noted that this purely empirical equation fits the experimental data better than the frequently used Arrhenius equation.[30] At room temperature, the viscosity is in the order of 5 Pa s, which means that this specific resin would need to be heated for use in VI processes, as otherwise fill times would be infeasibly long for practical application. For the purpose of this study, fill times are not a concern.

Measuring the viscosity of the resin as a function of the radiant exposure (at constant temperature) was not practical, as the degree of cure will not be uniform in a larger volume of irradiated resin as required for the viscometry. To estimate the time for the resin to gel (as an upper limit to the flow time), the degree of cure was quantified for different durations of irradiation via surface hardness measurement. A reinforcement specimen with dimensions 280 mm × 115 mm was first impregnated with resin and then positioned under the reflector housing of the UV lamp as shown in Figure 3. The specimen was divided into seven zones with a length $\Delta x = 40$ mm, which were exposed to UV irradiation for different durations (Figure 6). For each zone, the Barcol hardness was measured (ASTM D2583) as an indicator of the degree of cure, using a GYZJ 935 impresser (at room temperature). Measurement of the hardness on the top (directly exposed to irradiation) and bottom surface of the specimen allows quantification of the through-cure of the resin. Fifteen hardness values were sampled randomly on both surfaces (top and bottom) of each zone.

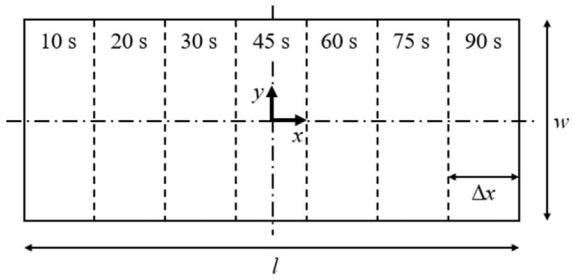

FIGURE 6 Different zones in specimen (with dimensions $\Delta x \times w$), irradiated for different durations

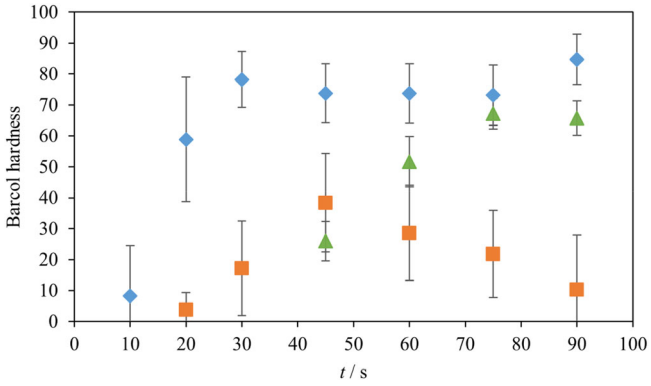

FIGURE 7 Barcol hardness as a function of irradiation time, t, on the top surface of specimen 1 (diamond markers), bottom surface of specimen 1 (square markers) and bottom surface of specimen 2 (triangular markers). Average values and standard deviations are indicated. The times relate to the zones indicated in Figure 6

This procedure was applied to two specimens. For specimen 1, the irradiation was started immediately after the resin flow front had reached the end of the specimen. For specimen 2, the feed line was clamped off and vacuum was applied for 15 min before the irradiation was started. Values of the measured hardness as a function of the irradiation time are plotted in Figure 7. In general, the scatter in hardness values for each zone is large. This is related to surface unevenness (particularly on the top surface) and the presence of randomly distributed fibers. The results show that cure is faster on the top surface than on the bottom surface of the specimen, because light transmission through the impregnated reinforcement is limited.

On the top surface of specimen 1 (diamond markers), the measured hardness increases with time and converges to a value in the order of 78, reflecting the dependence of the degree of cure on time expressed in Equations (3) and (4). After 10 s of irradiation, an average hardness value greater than zero was measured, indicating that the resin gels between 0 and 10 s of irradiation.

Extrapolating the hardness readings to a value of zero indicates that the surface provides resistance to indentation after approximately 9 s of irradiation. Here, this time is taken as an estimate for the point of gelation. The maximum hardness is reached after approximately 30 s. Any additional irradiation has no significant influence on the degree of cure. These observations were used to estimate H_0 in Equation (3).

On the bottom surface of specimen 1 (square markers), the resin is still liquid after 10 s of irradiation but is gelled after 20 s. Extrapolating the hardness readings to zero gives an estimate of 19 s for the gel point. Whilst the hardness as a function of time would be expected to show the same qualitative behavior as the hardness on the top surface, the measured hardness increases with increasing irradiation time, but then decreases for $t > 45$ s. The explanation can only be that the true radiant exposure (and the degree of cure) decreases for irradiation times longer than 45 s. As different irradiation times correspond to different zones of the specimen (Figure 6), the shape of the curve in Figure 7 implies that the irradiance was higher near the middle of the specimen (at intermediate irradiation times) than at the end of the specimen (at longer times).

Whilst the local irradiance on the top surface of the vacuum bag follows a parabolic profile (Figure 4), the systematic decrease in E from the middle (at $t = 45$ s) to the end (at $t = 90$ s) is smaller than the increase in irradiation time. Hence, this cannot explain a decrease in radiant exposure and the observed variations in hardness. Here, the local variation in hardness is related to variations in the specimen thickness. Before the resin infusion starts, a uniform pressure (atmospheric pressure) compacts the dry reinforcement in the vacuum bag. As the resin flow front propagates, the internal pressure increases in the saturated part of the reinforcement (to values between atmospheric pressure and vacuum pressure), resulting in local relaxation of the reinforcement compression and locally increasing thickness.[33] For specimen 1, this thickness variation was conserved as the specimen was cured immediately after the reinforcement was completely impregnated. The linear decrease in specimen thickness from 3.2 mm near the resin inlet (corresponding to an irradiation time of 90 s) to 1.8 mm near the vent (corresponding to 10 s) implies that the transmission of UV light decreases from the vent towards the inlet. Hence, the irradiance on the bottom surface decreases from the vent to the inlet, which explains the observed decrease in hardness towards the resin inlet (i.e., with increasing time).

For specimen 2, the hardness on the top surface converges to the same value as for specimen 1. For clarity, these data points are not indicated in Figure 7. Values on the bottom surface of specimen 2 are indicated by the triangular markers. The hardness increases continuously with increasing irradiation time and converges to the same value as the hardness on the top surface. For this specimen, the pressure distribution and thickness leveled out after the feed line was clamped off while vacuum was still applied. The thickness was 2.1 mm near the resin inlet (corresponding to an irradiation time of 90 s) and 1.9 mm near the vent (corresponding to 10 s). Hence, the irradiance on the bottom surface was approximately uniform, which implies that the radiant exposure increases linearly with increasing irradiation time and the degree of cure increases as described by Equations (3) and (4).

3.4 | Reinforcement properties

The in-plane permeability of the reinforcement was characterized experimentally at different values of V_f (in unsaturated radial flow experiments at constant injection pressure[34]). As the in-plane permeability has a small degree of anisotropy, it is approximated by an equivalent isotropic permeability,

$$K_{eq} = 1.01 \times 10^{-10}\,\mathrm{m}^2 V_f^{-1.39}. \tag{12}$$

The dependence of the fiber volume fraction on the compaction pressure, p_c, was determined experimentally for dry specimens, measuring the space between stiff and parallel compaction platens and the corresponding compaction force on a Universal Testing Machine (in compaction experiments at a relative speed of 1 mm/min between the platens). It can be approximated as

$$V_f = 0.23\left(\frac{p_c}{10^5\ \mathrm{Pa}}\right)^{0.19}. \tag{13}$$

4 | EXPERIMENTAL RESULTS AND DISCUSSION

4.1 | Reference experiments

For reference, two VI experiments were conducted at different temperatures with no UV irradiation (i.e., $H = 0$, $\eta = \text{const.}$), and the times for complete impregnation of the reinforcement were recorded:

- At a constant room temperature of 22°C (resin and tool surface), the time for complete impregnation of the reinforcement was approximately 24 min (1440 s).
- At a measured temperature of approximately 43°C, the time for complete impregnation was 320 s. Here, the

TABLE 3 Reference experiments: Calculated time and experimental time for complete impregnation, t_c and t_e, and relative difference $(t_e - t_c)/t_c$, for two different temperatures, T

T (°C)	t_c (s)	t_e (s)	$(t_e - t_c)/t_c$ (%)
22	1660	1440	−13
43	264	320	18

resin container was preheated, and the infusion was carried out on a heated tool surface. Using a non-contact infrared thermometer, the temperature was measured on the surface of the vacuum bag during the infusion.

For uni-directional flow at constant viscosity, Equation (7) can be integrated to find the time for the flow front to propagate by a distance x_f,

$$t = \frac{\eta \Phi}{2K\Delta p} x_f^2. \tag{14}$$

For complete impregnation of the reinforcement specimen, x_f corresponds to the total length, $l = 0.28$ m. The flow-driving pressure difference is $\Delta p = 10^5$ Pa. For the reinforcement used here, Equation (13) indicates that the value of Φ is approximately 0.77 at a compaction pressure of 10^5 Pa. According to Equation (12), the corresponding permeability is approximately $K_{eq} = 8 \times 10^{-10}$ m^2, which is substituted for K. This approximation ignores that the reinforcement thickness, and hence porosity and permeability, can vary with position and time in VI. The viscosity of the uncured resin is approximately 4.4 Pa s at $T = 22$°C and 0.7 Pa s at $T = 43$°C. Using Equation (14) and the values for η, Φ, K_{eq}, Δp, and l given above, fill times of 1660 and 264 s can be calculated for the two temperatures. Comparison of calculated and experimental fill times in Table 3 shows that relative differences for both temperatures are smaller than 20%, which indicates that the results from the infusion experiments are consistent with the measured dependence of the resin viscosity on the temperature. Here, it is to be considered that the parameters are hard to control accurately in VI processes, and that porosity and permeability can vary during the infusion. Hence, the flow behavior is expected to show a relatively high variability.

4.2 | Combined effect of temperature and cure

To study the combined effect of global viscosity reduction though heating and local viscosity increase through curing, infusions were conducted at two temperatures with localized UV irradiation (from the beginning of the infusion). Here, the specimens were rectangular with dimensions 140 mm × 115 mm. The infusion set-up was the same as above. A cardboard mask with the dimensions indicated in Figure 8A was used to cover the surface of the reinforcement specimens in three rectangular areas with different lengths, l_m. These areas were separated by rectangular gaps, where the reinforcement was exposed to irradiation. The measured resin temperatures for the experiments were $T = 20$°C and $T = 43$°C. Resin was infused until it was estimated (based on the reference experiments) that the flow front would have reached the end of the specimens. Then, the feed line was clamped off, and the cardboard mask was removed so that the resin was cured everywhere in the impregnated part of the reinforcement.

In the specimens infused and cured at both temperatures, the flowing resin gels so fast on the top surface of the irradiated area that the flow front does not propagate beyond the edges of the mask (Figure 8B). On the bottom surface, resin gelation is delayed because of the limited UV transmission through the reinforcement. Hence, the resin can flow beyond the edges of the mask before it gels (Figure 8C). The flow length in the irradiated part of the specimen, Δx_f, was measured for each covered rectangular area (Figure 9) as a measure for the accuracy of controlling the flow front propagation. The values of Δx_f decrease with increasing l_m (i.e., the accuracy of control increases), as the effective pressure drop at the edge of the mask decreases with increasing distance from the resin inlet. They increase with increasing temperature (i.e., the accuracy decreases), as this means that the flow velocity prior to gelation is increased. Both observations are qualitatively consistent with the results from the numerical solution of the flow equation (Section 2.3). However, the estimate for c in Table 1 does not consider through-thickness variations in irradiance. Hence, values of Δx_f from the numerical solution (Figure 2) are not a quantitatively accurate representation of the experimental observations on the top or bottom surface (Figure 9).

4.3 | Racetracking

To assess whether racetracking can be suppressed using local UV irradiation, infusion experiments were carried out at room temperature. Unlike in the reference experiments, a channel with a width of approximately 10 mm was created along one long edge of the reinforcement using flow mesh (four layers).

In an experiment without UV irradiation (case 1), the resin flow front propagates faster in the channel than in

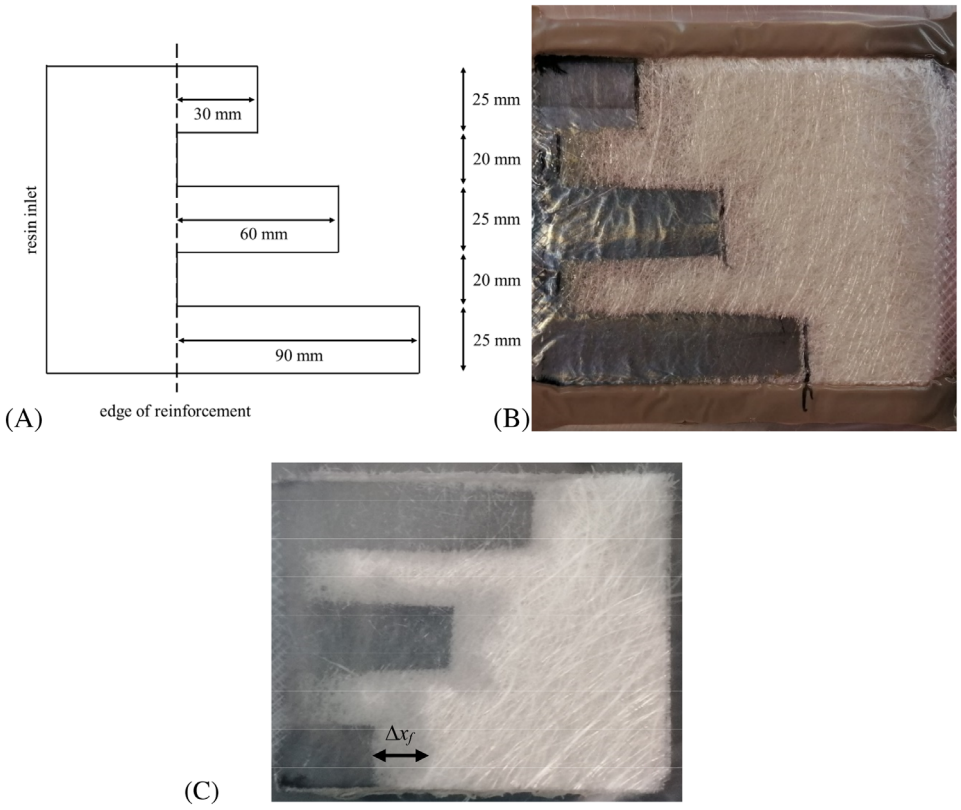

FIGURE 8 Vacuum infusion experiments with UV irradiation; reinforcement covered with a mask; (A) geometry of mask; (B) impregnated specimen after removal of mask ($T = 20°C$, top surface); (C) impregnated specimen after removal of mask ($T = 20°C$, bottom surface)

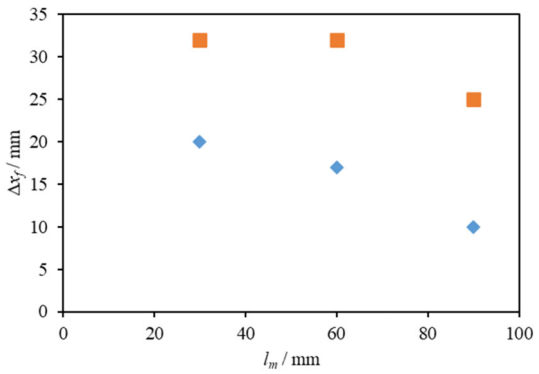

FIGURE 9 Length of flow beyond the end of the mask, Δx_f, on bottom surface of specimen for rectangular covered areas with lengths, l_m; infusions at $T = 20°C$ (diamond markers) and at $T = 43°C$ (square markers)

the reinforcement, as the permeability of the flow mesh is greater than the permeability of the reinforcement (racetracking). A transverse pressure gradient develops, which results in a curved flow front shape as resin flows from the channel into the reinforcement.[5] The photograph in Figure 10A was taken before the resin in the channel reached the end of the specimen. The flow front positions relative to the resin inlet, that is, the distances covered by the flow front, x_{fi}, are given in Table 4. Here, $i = 1$ relates to the reinforcement, $i = 2$ to the channel. The difference between the flow front positions in the flow channel and at the left edge of the reinforcement, $x_{f2} - x_{f1}$, was 169 mm.

Using the same set-up, two cases with UV irradiation were studied:

- For case 2, the reinforcement was covered with a cardboard mask, such that only the channel was exposed to irradiation. Hence, the width of reinforcement exposed to irradiation was approximately 0 mm (Figure 10B).
- For case 3, the channel and a strip of reinforcement with a width of approximately 10 mm were exposed to irradiation (Figure 10C).

In both cases with UV irradiation, the flow front in the reinforcement is approximately straight. Minor deviations can be seen near the left edge (in Figure 10B,C), where the reinforcement compaction is not quite uniform as the sealant tape used for vacuum bagging has a different thickness. Unlike in case 1, the flow in the channel is separated from the flow impregnating the reinforcement. After an infusion time of 5 min (when the photographs in Figure 10B,C were taken), the flow front position in the channels, x_{f2}, is 74 mm and 78 mm, while the average flow front position in the reinforcement, x_{f1}, is 135 mm and 149 mm, respectively (Table 4). Results for cases 2 and 3 are consistent, considering unavoidable uncertainties in the vacuum bag lay-up. This indicates that the

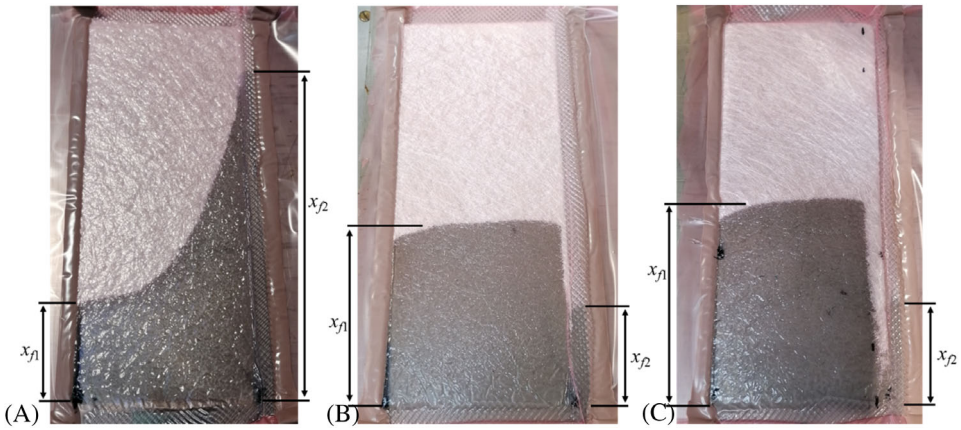

FIGURE 10 Vacuum infusion experiments with racetracking; (A) no UV irradiation; (B) UV irradiation on racetracking channel only (reinforcement exposed on a width of approx. 0 mm); (C) UV irradiation on racetracking channel and reinforcement on a width of approx. 10 mm; x_{f1} and x_{f2} indicate flow front positions in reinforcement and in flow channel, respectively

TABLE 4 Observations from experiments with racetracking, corresponding to Figure 8: Flow front positions in the reinforcement, x_{f1}, and in the channel, x_{f2}, at different infusion times, t

Case	t (s)	x_{f1} (mm)	x_{f2} (mm)
1: no control		74 (left edge)	243
2: 0 mm gap width	300	135 (average)	74
3: 10 mm gap width	300	149 (average)	78

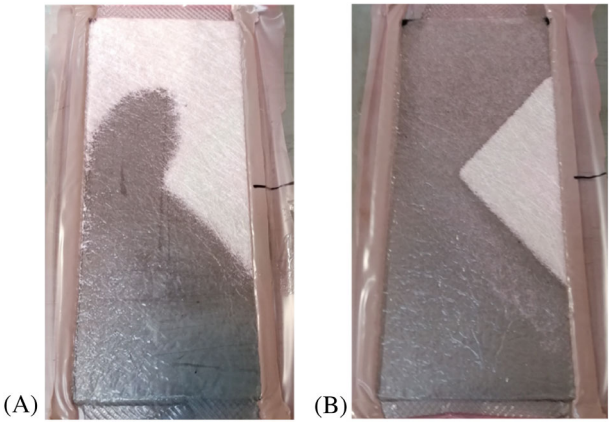

FIGURE 11 Vacuum infusion experiments with UV irradiation, reinforcement covered with a mask with triangular cut-out; (A) mask removed before impregnation was complete; (B) mask removed after complete impregnation

width of the irradiated reinforcement material does not have a significant effect on the result. It can be concluded that suppressing racetracking by stopping flow in the channel through the change in viscosity and gelation is feasible.

In cases 2 and 3, the edge of the mask separating the covered reinforcement from the exposed channel (right edge in Figure 10) is parallel to the direction of the applied pressure gradient. Transverse pressure gradients develop as a result of different flow front propagation in the channel and the reinforcement. As long as the flow front propagation is faster in the channel than in the reinforcement, there is transverse flow from the channel into the reinforcement. As the resin in the channel gels quickly, only a small amount can flow into the reinforcement. Once the flow front in the reinforcement has passed the position of the stalled resin flow front in the channel, x_{f2}, resin tends to flow from the reinforcement towards the channel (in a reversal of racetracking). However, this effect is small as transverse pressure gradients and fluid exchange decrease from the resin inlet towards the flow front.

For case 3, it can be seen in Figure 10C that only a small amount of resin flows transversely into the 10 mm wide exposed strip of reinforcement (near the resin inlet), mainly on the bottom surface of the specimen. For case 2, limited accuracy of reinforcement cutting and application of masks means that the width of the exposed reinforcement may not exactly be 0 mm. A very narrow strip of dry reinforcement separating the impregnated reinforcement and the empty channel helps to minimize transverse flow. Hence, flow in the reinforcement and racetracking channel is separated clearly.

4.4 | Different flow patterns

Experiments were carried out at room temperature, using the same infusion geometry as in the reference experiments. For one example, the reinforcement was covered with a cardboard mask (with a triangular cut-out), such that only a triangular area along the right edge was exposed to UV light. Figure 11 shows that a converging–diverging flow develops during the infusion process. In the experiment shown in Figure 11A, the mask was removed before the flow front had reached the end of the reinforcement. As the viscosity increased, the flow stopped, and the reinforcement impregnation remained

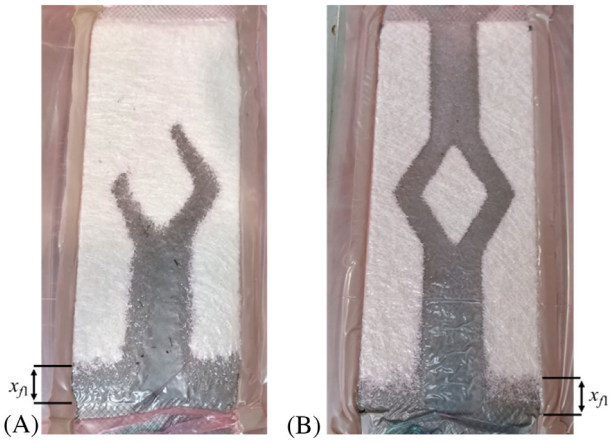

FIGURE 12 Vacuum infusion experiments with UV irradiation; reinforcement covered with a mask (strip along flow direction, with rhombic inclusion); (A) mask removed before impregnation was complete; (B) mask removed after complete impregnation

incomplete. Figure 11B shows a complete impregnation. It is to be noted that the boundaries between dry and impregnated reinforcement are well defined. As the pressure drop is significantly reduced (compared to the start of the infusion) when the flow front crosses the boundary between masked and exposed reinforcement, the distance traveled by the fluid in the exposed area is very short (see Figure 2). As the edges of the mask at the cut-out are at angles of $\pm 45^\circ$ relative to the direction of the applied pressure gradient, this deviation from the masked shape is further reduced by a factor of 0.7. On the bottom surface of the specimens, the flow front traveled a distance in the order of 4 mm (perpendicular to the edge of the mask) in the exposed area. This deviation was observed only on the side of the triangle nearer to the resin inlet, where the effective flow width reduces.

In a second example, most of the reinforcement was exposed to UV light. Using a cardboard mask, a narrow flow path with a rhombic inclusion was created along the axis of the geometry. Figure 12 shows that splitting and merging flow fronts develop during the resin infusion. In the experiment shown in Figure 12A, the flow was stopped by removing the mask, such that the reinforcement impregnation remained incomplete. Here, the flow pattern is not symmetrical, which is related to the local non-uniformity of the permeability of the random fiber material. In Figure 12B, the reinforcement impregnation is complete, and effects of local permeability variations are not noticeable.

At the resin inlet, the pressure gradient is perpendicular to the edge of the mask (bottom edge of the specimen in Figure 12). At the start of the infusion, the pressure gradient has a high value (Δp is given, and x_f is still approximately zero). Hence, the resin can cover a relatively long distance in the unmasked area of the reinforcement before it gels and the flow stops. The average flow lengths in the unmasked part of the reinforcement, x_{f1}, are approximately 26 mm (Figure 12A) and 20 mm (Figure 12B), respectively. These values of x_{f1} are observed on the bottom surface of the cured specimen. Where the edges of the mask are parallel to the direction of the applied pressure gradient, the maximum distance covered by the flow front in the exposed area is approximately 6 mm (near the inlet, on the bottom surface).

5 | CONCLUSION

Composite specimens from a random glass filament mat and a UV-curable acrylic modified polyester resin were produced in a VI process. During the reinforcement impregnation, the resin viscosity was increased selectively through localized irradiation with UV light to control the resin flow and to realize different flow patterns. Here, opaque cardboard masks were used to create defined irradiation patterns. This approach is based on radical photopolymerisation, where the resin cures only under direct irradiation and remains uncured in areas covered with a mask. Hence, the viscosity of the flowing resin is constant in masked areas. It increases in areas exposed to UV light until the resin gels and the flow stalls in a matter of seconds.

Theoretical considerations show that the distance covered by the moving resin flow front in exposed areas prior to resin gelation decreases with increasing UV irradiance, decreasing applied pressure gradient and decreasing resin temperature. In experiments, the resin flow front did not propagate beyond the boundaries of the masked areas on the top surface of the specimens. On the bottom surface, resin was observed to flow into irradiated areas, where it covered distances in the order of 10 mm. As the transmission of UV light through the impregnated glass fiber reinforcement is limited, the irradiance is lower on the bottom surface than on the top surface of a specimen. As a result, the time for resin gelation is longer and the flow front propagates further on the bottom surface than on the top surface. Because of the dependence on the pressure gradient, flow lengths in the irradiated area decrease with increasing distance from the resin inlet.

Despite the minor uncertainties in the flow patterns on the bottom surface, it was possible to steer the flow along converging–diverging paths with inclusions and to suppress racetracking along reinforcement edges. Practical applications of the process studied here could be in process control, that is, compensation for local variations

in fiber volume fraction and permeability of fibrous reinforcements. Selection of other combinations of suitable resin systems and UV light sources may help to optimize the process. Its applicability is limited by the requirement for UV transparency of the reinforcement and the tool. It would need to be considered in process planning that the photocuring process is irreversible.

ACKNOWLEDGMENT

This work was supported by the Engineering and Physical Sciences Research Council, UK, through the EPSRC Future Composites Manufacturing Research Hub [EP/P006701/1].

DATA AVAILABILITY STATEMENT

The data that support the findings of this study are available from the corresponding author upon reasonable request.

ORCID

Andreas Endruweit https://orcid.org/0000-0002-1776-175X

REFERENCES

[1] B. R. Gebart, *J. Compos. Mater.* **1992**, *26*(8), 1100.
[2] M. Bodaghi, S. V. Lomov, P. Simacek, N. C. Correia, S. G. Advani, *Compos. Part A: Appl. Sci. Manuf.* **2019**, *120*, 188.
[3] P. Smith, C. D. Rudd, A. C. Long, *Compos. Sci. Technol.* **1997**, *57*(3), 327.
[4] A. Endruweit, X. Zeng, A. C. Long, *Adv. Manuf.: Polym. Compos. Sci.* **2015**, *1*(1), 3.
[5] S. Bickerton, S. G. Advani, *Compos. Sci. Technol.* **1999**, *59*(15), 2215.
[6] J. Ni, Y. Zhoa, L. J. Lee, S. Nakamura, *Polym. Compos.* **1997**, *18*(2), 254.
[7] S. Bickerton, S. E. M. Sozer, P. J. Graham, S. G. Advani, *Compos. Part A: Appl. Sci. Manuf.* **2000**, *31*(5), 423.
[8] P. Barooah, B. Berker, J. Q. Sun, *J. Manuf. Sci. E.-Trans. ASME* **2001**, *123*(2), 240.
[9] A. Gokce, S. G. Advani, *J. Manuf. Sci. E.-Trans. ASME* **2003**, *125*(3), 548.
[10] O. Restrepo, K. T. Hsiao, A. Rodriguez, B. Minaie, *Compos. Part A: Appl. Sci. Manuf.* **2007**, *38*(6), 1547.
[11] M. Y. Matveev, A. Endruweit, A. C. Long, M. A. Iglesias, M. V. Tretyakov, *Compos. Part A: Appl. Sci. Manuf.* **2021**, *143*, 106323.
[12] D. Modi, N. Correia, M. Johnson, A. Long, C. Rudd, F. Robitaille, *Compos. Part A: Appl. Sci. Manuf.* **2007**, *38*(5), 1271.
[13] A. R. Nalla, M. Fuqua, J. Glancey, B. Leleiver, *Compos. Part A: Appl. Sci. Manuf.* **2007**, *38*(3), 1058.
[14] J. B. Alms, S. G. Advani, J. L. Glancey, *Compos. Part A: Appl. Sci. Manuf.* **2011**, *42*(1), 57.
[15] M. Poorzeinolabedin, K. L. Parnas, *Adv. Manuf.* **2019**, *7*(2), 199.
[16] R. J. Johnson, R. Pitchumani, *Compos. Sci. Technol.* **2003**, *63*(15), 2201.
[17] R. Matsuzaki, S. Kobayashi, A. Todoroki, Y. Mizutani, *Compos. Part A: Appl. Sci. Manuf.* **2011**, *42*(7), 782.
[18] A. Endruweit, M. S. Johnson, A. C. Long, *Polym. Compos.* **2006**, *27*(2), 119.
[19] C. Decker, *Prog. Polym. Sci.* **1996**, *21*(4), 593.
[20] A. W. Green, *Industrial Photoinitiators – A Technical Guide*, CRC Press, Boca Raton, FL **2010**.
[21] M. Livesay, in: *Proceedings of Composites '97*, Anaheim **1997**, https://0201.nccdn.net/1_2/000/000/130/16e/smeana.pdf (accessed: January 16, 2022).
[22] Q. Yuan, M. B. Yang, Y. W. Mai, *Adv. Compos. Lett.* **2000**, *9*(5), 341.
[23] A. O. Nwabuzor, O. I. Okoli, in: *Proceedings of Composites 2004*, Tampa **2004**.
[24] W. Carroll, H. Nava, in: *Proceedings of Composites 2004*, Tampa **2004**.
[25] E. Lackey, K. Inamdar, L. Worrel, W. Al-Akhdar, D. A. Wostratzky, *RadTech Rep.* **2001**, *15*, 36.
[26] S. Adanur, Y. Arumugham, *J. Ind. Text.* **2002**, *32*(2), 93.
[27] S. Adanur, Y. Arumugham, *J. Ind. Text.* **2002**, *32*(2), 107.
[28] K. C. Kennedy II, R. P. Kusy, *J. Vinyl Addit. Technol.* **1995**, *1*(3), 182.
[29] Y. C. Chen, J. L. Ferracane, S. A. Prahl, *Dent. Mater.* **2005**, *21*(11), 1075.
[30] M. B. Roller, *Polym. Eng. Sci.* **1986**, *26*(6), 432.
[31] D. S. Lee, C. D. Han, *Polym. Eng. Sci.* **1987**, *27*(13), 955.
[32] A. Endruweit, W. Ruijter, M. S. Johnson, A. C. Long, *Polym. Compos.* **2008**, *29*(7), 818.
[33] N. C. Correia, F. Robitaille, A. C. Long, C. D. Rudd, P. Šimáček, P. S. G. Advani, *Compos. Part A: Appl. Sci. Manuf.* **2005**, *36*(12), 1645.
[34] A. Endruweit, P. McGregor, A. C. Long, M. S. Johnson, *Compos. Sci. Technol.* **2006**, *66*(11–12), 1778.

How to cite this article: A. Endruweit, M. Matveev, M. V. Tretyakov, *Polym. Compos.* **2022**, 1. https://doi.org/10.1002/pc.27001